

Planet Formation around Super Massive Black Holes in the Active Galactic Nuclei

KEIICHI WADA,^{1,2,3} YUSUKE TSUKAMOTO,¹ AND EIICHIRO KOKUBO⁴

¹*Kagoshima University, Graduate School of Science and Engineering, Kagoshima 890-0065, Japan*

²*Ehime University, Research Center for Space and Cosmic Evolution, Matsuyama 790-8577, Japan*

³*Hokkaido University, Faculty of Science, Sapporo 060-0810, Japan*

⁴*National Astronomical Observatory of Japan, Mitaka 181-8588, Japan*

ABSTRACT

As a natural consequence of the elementary processes of dust growth, we discovered that a new class of planets can be formed around supermassive black holes (SMBHs). We investigated a growth path from sub-micron sized icy dust monomers to Earth-sized bodies outside the “snow line”, located several parsecs from SMBHs in low luminosity active galactic nuclei (AGNs). In contrast to protoplanetary disks, the “radial drift barrier” does not prevent the formation of planetesimals. In the early phase of the evolution, low collision velocity between dust particles promotes sticking; therefore, the internal density of the dust aggregates decreases with growth. When the porous aggregate’s size reaches 0.1–1 cm, the collisional compression becomes effective, and the decrease in internal density stops. Once 10–100 m sized aggregates are formed, they are decoupled from gas turbulence, and the aggregate layer becomes gravitationally unstable, leading to the formation of planets by the fragmentation of the layer, with ten times the mass of the earth. The growth time scale depends on the turbulent strength of the circumnuclear disk and the black hole mass M_{BH} , and it is comparable to the AGN’s lifetime ($\sim 10^8$ yr) for low mass ($M_{BH} \sim 10^6 M_{\odot}$) SMBHs.

1. INTRODUCTION

Planetary systems are ubiquitous – more than four thousand exoplanets have been discovered thus far¹. However, protoplanetary disks around stars may not be the only site for planet formation in the universe. Here we propose a new site of “planet” formation: the circumnuclear disk around supermassive black holes (SMBHs).

Most galaxies host SMBHs at their centers, with masses ranging from a few million to billion solar masses. Gas disks around SMBHs emit large amount of energy owing to mass accretion onto the SMBHs, which are known as the “central engine” of active

Corresponding author: Keiichi Wada
wada@astrophysics.jp

¹ <https://exoplanetarchive.ipac.caltech.edu/>

Table 1. Differences between the proto-planetary disk and AGN.

	proto-planetary disk	circumnuclear disk
mass of the central object	$M_{\star} \sim M_{\odot}$	$M_{BH} \sim 10^{6-9} M_{\odot}$
luminosity of the central source	$\sim L_{\odot}$	$10^{10-12} L_{\odot}$
spectrum of the central source	black body	power law
size of the dusty disk	10-100 AU	0.1 pc - 100 pc
inner edge of the dusty disk	~ 0.1 pc ^a	dust sublimation radius (sub pc \sim pc)
gas mass	$\sim 0.01 M_{\star}$	$\sim 0.1 M_{BH}$
dust mass	$\sim 10^{-4} M_{\odot}$	$\sim 10^3 - 10^6 M_{\odot}$
rotational period	~ 100 yr	$\sim 10^6 - 10^8$ yr
life time	$\sim 10^6$ yr	$10^7 - 10^8$ yr
drag law	Epstein/Stokes	Epstein
mean free path of gas	$\sim 1-100$ cm	$\sim 10^{12} (\frac{n}{10^3 \text{ cm}^{-3}})^{-1}$ cm

^a Eisner et al. (2007); Suzuki et al. (2010)

galactic nuclei (AGNs). It is believed that the mass of SMBH in a galaxy depends on its host galaxy’s bulge mass (Marconi, & Hunt 2003). Researchers are more convinced of the presence of SMBHs since the discovery of the “black hole shadow” in M87 (Event Horizon Telescope Collaboration et al. 2019). In the “unified model” of AGNs (Antonucci 1993; Netzer 2015), the gas and dust form a geometrically and optically thick “torus”, and it obscures the broad emission line (line width is several 1000 km s^{-1}) region around the central accretion disk. This hypothesis successfully explains the type-1 and type-2 dichotomy of Seyfert galaxies’ spectra, depending on the viewing angle of the tori. The real structure of the tori has been unclear for many years. Recently, the Atacama Large Millimeter/sub millimeter Array (ALMA) spatially resolved the molecular tori in nearby AGNs (García-Burillo et al. 2016; Imanishi et al. 2018; Izumi et al. 2018; Combes et al. 2019). Their internal structure is still not well resolved; however, recent 3-D radiation-hydrodynamic simulations suggested a dynamic structure energized by a radiation-driven fountain flow to sustain their geometrical thickness (Wada 2012; Wada et al. 2018, see also Fig. 1). Notably, even in this situation, cold, dense gas forms a geometrically thin disk (Schartmann et al. 2014; Wada et al. 2016), and this stratified structure is also consistent with recent X-ray surveys (Buchner et al. 2014).

The remainder of this paper is organized as follows. In §2, we describe dust and its environment around SMBHs, and their differences from the standard situation, i.e. in the circum-stellar disks. In §3, we show a typical evolutionary track of a representative dust particles from a monomer to a planet-sized body. Four stages of the dust coagulation based on the recent theoretical model proposed for the proto-planet disks are described in details in Appendix. We also discuss how the evolutionary time scales depend on parameters in §5.

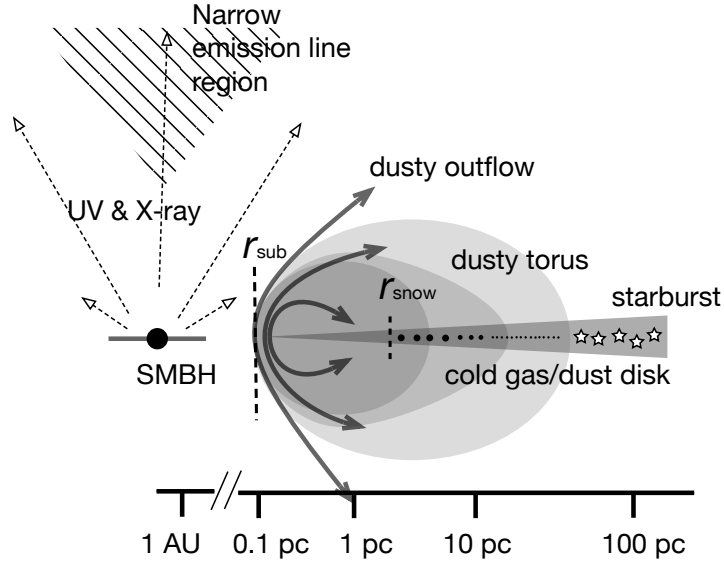


Figure 1. A schematic picture of the Active Galactic Nucleus (AGN) and the circumnuclear disk. A supermassive black hole (the mass is $10^6 - 10^9 M_\odot$) is surrounded by an accretion disk, which radiates enormous energy ($\sim 10^{42} - 10^{45} \text{ erg s}^{-1}$) mostly in the ultra-violet and X-ray. The dust particles in the central $r < r_{\text{sub}} \sim 0.1$ - a few parsecs are sublimated owing to the heating by the central radiation. The radiation forms conical ionized gas (Narrow emission-line region) and also contributes to producing outflows of the dusty gas and torus (Wada 2012; Wada et al. 2018; Izumi et al. 2018). In the mid-plane of the torus, cold, dense gas forms a thin disk, where icy dust particles can present beyond the snow-line r_{snow} . The dust aggregates evolve by collisions to form planetesimals, and eventually “circum-black hole planets” by the gravitational instability of the aggregate disk.

2. ENVIRONMENT OF DUST AROUND AGNS IN COMPARISON WITH PROTO-PLANETARY DISKS

2.1. The snow line in AGNs and major difference from the proto-planetary disks

The dusty gas around SMBHs extends beyond the dust sublimation radius r_{sub} , where the dust temperature is higher than the sublimation temperature of the dust grains ($T_{\text{sub}} \sim 1500 \text{ K}$). The radius depends on the AGN luminosity: $r_{\text{sub}} = 1.3 \text{ pc} \left(\frac{L_{\text{UV}}}{10^{43} \text{ erg s}^{-1}} \right)^{0.5} \left(\frac{T_{\text{sub}}}{1500 \text{ K}} \right)^{-2.8} \left(\frac{a_d}{1 \mu\text{m}} \right)^{-1/2}$, where L_{UV} is the ultra-violet luminosity of the AGN, and a_d is the dust size (Barvainis 1987). The temperature of the gas and dust beyond r_{sub} , especially at the mid-plane of the dusty torus, should be cold $\lesssim 100 \text{ K}$ (Schartmann et al. 2014), because the radiation originated from the accretion disk is weaker in the direction of the disk plane, and it is further attenuated by the dense dusty gas. Interestingly, even for X-rays, a large fraction of AGNs are Compton-thick, i.e. the Hydrogen column density is $N_H > 10^{24} \text{ cm}^{-2}$ (Buchner et al. 2014). Although near-infrared and mid-infrared interferometer observations of AGNs show the presence of hot dusts (several 100 K) around AGNs (Tristram et al. 2014), colder dust particles are also present in this dense media around AGNs. The

total amount of dust in the central 6-27 pc around SMBHs estimated from recent molecular lines (e.g. CO) observations of nearby AGNs by ALMA (Combes et al. 2019) is enormous, e.g. $\sim 0.7 - 3.9 \times 10^5 M_\odot$ for the dust-to-gas mass ratio of ~ 0.01 (Draine 2011). This number could be even larger for the high metallicity environment around AGNs (Groves et al. 2006; Rémy-Ruyer et al. 2014). The internal dynamics and structure of the molecular tori are still observationally unclear. However, since the mass feeding to the AGN through the circumnuclear disk is necessary during their lifetime ($\sim 10^7 - 10^8$ yr), the turbulent viscosity works in the dusty gas disk. Here, we model the turbulent disk based on the α -viscosity formalism (Shakura, & Sunyaev 1973; Shlosman, & Begelman 1987).

The dust grains in the circumnuclear disks around SMBHs are in a qualitatively similar situation as the ones in proto-planetary disk. The major difference between the two systems are summarized in Table 1. The “snow line” for $a_d = 0.1 \mu m$ dust irradiated by X-ray around an AGN with a SMBH of $10^7 M_\odot$ for the Eddington ratio (γ_{Edd}) of 0.1 is

$$r_{snow} \approx 4.7 \text{ pc} (L_X / 1.3 \times 10^{42} \text{ erg s}^{-1})^{1/2} (T_{ice} / 170 \text{ K})^{-2.8} a_{d,0.1}^{-1/2} \quad (1)$$

(Barvainis 1987)². Moreover, AGNs are often heavily obscured (Compton-thick) even for hard-X rays (Buchner et al. 2014), suggesting that a cold dusty layer exists around SMBHs. Therefore, it is expected that the dust in the most part of the circumnuclear disk is icy.

2.2. Outline of evolution of “fluffy” dust aggregates

We then apply recent models of coagulation of dust particles and their aggregates outside the snow line in the protoplanetary disk (Okuzumi et al. 2012; Kataoka et al. 2013; Suyama et al. 2012; Michikoshi, & Kokubo 2016, 2017) to the dust around AGNs. The coagulation of ‘fluffy icy dust’ is one of the plausible solutions to avoid the theoretical obstacles that prevent from growth of dust grains (monomers) to “planetesimal” such as the “radial drift barrier” (Okuzumi et al. 2012). In this scenario, the evolution of the dust can be divided into four stages: 1) “hit-and-stick” phase, 2) collisional or gas pressure compression phase, 3) gravitationally compression phase, and 4) gravitational instability phase (e.g. Goldreich, & Ward 1973). We investigated each phase in the circumnuclear disk as discussed below (see also Appendix).

We track the evolution of icy monomers, whose size and density are $a_0 = 0.1 \mu m$ and $\rho_0 = 1 \text{ g cm}^{-3}$, and their aggregates. Here, we investigate the evolution of a representative dust particle size, using the single-size approximation (Sato et al. 2016). In the hit-and-stick phase, when two monomers/aggregates collide, the internal structure of the aggregates becomes porous (i.e. average internal density is smaller than ρ_0) with internal voids (Suyama et al. 2012). This “fluffy dust” formation is also

² The approximate proportionality $a_d^{-1/2}$ comes from the absorption efficiency of a dust grain being roughly proportional to its radius at a certain wavelength in the near-IR (Draine, & Lee 1984).

examined by numerical experiments (Dominik, & Tielens 1997; Wada et al. 2008). The internal density and size of the aggregates are $\rho_{int} \sim (m_d/m_0)^{-1/2} \rho_0$ and $a_d \sim (m_d/m_0)^{1/2} a_0$, where m_d and m_0 are the masses of the aggregate and monomers, for the fractal dimension of 2. When the collision energy exceeds a critical value, the porous aggregates start to get compressed, and the evolution of the internal density changes beyond this point (Suyama et al. 2012). During this compression phase, the aggregates' mass rapidly increase; however, their internal densities gradually increase as well, from $\rho_{int} \sim 10^{-6} \text{ g cm}^{-3}$ to $\sim 10^{-4} \text{ g cm}^{-3}$.

In contrast to the dust coagulation process in the protoplanetary disks (Weidenschilling 1977), the drag between dust particles and gas obeys the Epstein law only. The aggregate's size (a_d) is always much smaller than the mean free path of the gas ($\lambda_{mfp} \sim 10^{12} \text{ cm} \left(\frac{\sigma_{mol}}{10^{-15} \text{ cm}^2}\right)^{-1} \left(\frac{n_{mol}}{10^3 \text{ cm}^{-3}}\right)^{-1}$, where σ_{mol} and n_{mol} are the collisional cross-section and number density of the gas). At all times the radial drift velocity of the dust is negligibly small compared to the Kepler velocity v_K (i.e. $10^{-4} - 10^{-5} v_K$).

In both the protostellar and the circumnuclear disks, the dust-gas coupling is characterized by the normalized stopping time, i.e., the Stokes number, $S_t \equiv \Omega_K t_{stop}$, where t_{stop} is the time scale of the dust particles to reach the terminal velocity due to the gas drag. In the Epstein law, t_{stop} is proportional to $\rho_{int} a_d$, then S_t is

$$\begin{aligned} S_t &= \frac{\pi \rho_{int} a_d}{2 \Sigma_g} \\ &= \frac{\pi \rho_{int} a_d (\pi G Q_g)}{2 c_s \Omega_K} \\ &\sim 1.5 \times 10^{-5} \rho_{int,1} a_{d,0.1} c_{s,1}^{-1} r_1^{3/2} M_{BH,6}^{-1/2} Q_g, \end{aligned} \quad (2)$$

where Q_g is the Toomre's Q-value for a gas disk and $Q_g \equiv c_s \Omega_K / (\pi G \Sigma_g)$, with the surface density of the gas disk Σ_g , and $a_{d,0.1} \equiv a_d / (0.1 \mu m)$, the sound velocity of the gas $c_{s,1} = c_s / (1 \text{ km s}^{-1})$ and $\rho_{int,1} \equiv \rho_{int} / (1 \text{ g cm}^{-3})$. $Q_g < 1$ is a necessary condition for the ring-mode gravitational instability.

The radial velocity of the dust $v_{r,d}$ relative to the gas (Weidenschilling 1977; Tsukamoto et al. 2017) is

$$v_{r,d} = \frac{2S_t}{1 + S_t^2} \eta v_K, \quad (3)$$

where η is a parameter that determines the sub-Keplerian motion of the gas,

$$\eta \equiv -\frac{1}{2} \frac{c_s^2}{v_K^2} \frac{d \ln P}{d \ln r} \sim 2 \times 10^{-5} M_{BH,7}^{-1} c_{s,1}^2, \quad (4)$$

where $M_{BH,7} \equiv M_{BH} / 10^7 M_\odot$. Therefore, both in the early stage of the dust evolution ($S_t \ll 1$) and in the late phase ($S_t \sim 1$) in the circumnuclear disk, $v_{r,d}$ is much smaller than v_K , then we can ignore the radial drift of the aggregates in the circumnuclear disk during the whole evolution. The ‘‘radial drift barrier’’, i.e. the dust growth is limited by infalling to the central stars before dust particles obtain large enough mass as planetesimals, is not a serious problem in the circumnuclear disk.

2.3. The Growth time and destruction by collisions

The growth time of the aggregate during the hit-and-stick phase can be estimated as in Tsukamoto et al. (2017):

$$\begin{aligned}
 t_{grow} &\equiv (d \ln m_d / dt)^{-1} \\
 &= \frac{4\sqrt{2\pi} H_d \rho_{int} a_d}{3 \Delta v \Sigma_d} = \frac{8(2\pi)^{3/2}}{3} \frac{H_g}{\sqrt{\alpha} R_e^{1/4} c_s f_{dg}} \\
 &\sim 6.3 \times 10^7 \text{ [yr]} c_{s,1}^{-1} \left(\frac{f_{dg}}{0.01} \right)^{-1} \left(\frac{H_g}{0.1 \text{ pc}} \right) \left(\frac{\alpha}{0.1} \right)^{-1/2} \left(\frac{R_e}{10^4} \right)^{-1/4} \quad (5)
 \end{aligned}$$

where, f_{dg} is the dust-to-gas ratio and H_d and H_g are scale heights of dust and gas disks, and $H_d \approx H_g \propto M_{BH}^{-1/2} r^{3/2}$ in the circumnuclear disk. The Reynolds number R_e and the relative velocity of the dust particles Δv are given in Appendix. This growth time is comparable to the AGN life time (see §3 and Appendix in more details).

During the dust compression phase due to collisions, the kinematics of the dust aggregates are dominated by eddies of turbulence in the gas disk. Therefore, relative velocity of the aggregates, Δv , which is important for both growth and destruction of them, is determined by the property of the turbulence, i.e., R_e , and S_t (Ormel, & Cuzzi 2007). The dimensionless parameter α is a parameter to determine the kinematic viscosity in the turbulent disk (Shakura, & Sunyaev 1973):

$$\alpha \equiv \frac{\dot{M}_g}{3\pi \Sigma_g c_s^2 / \Omega_K} = \frac{\dot{M}_g G}{3c_s^3} Q_g \simeq 0.3 Q_g \left(\frac{\gamma_{Edd,6}}{0.01} \right) c_{s,1}^{-3}, \quad (6)$$

where \dot{M}_g is the radial mass accretion rate in the disk, and $\gamma_{Edd,6}$ is the Eddington rate for the BH mass with $M_{BH} = 10^6 M_\odot$ for the energy conversion efficiency of 0.1. Here, we assume α is a constant, smaller than unity throughout the disk. In this phase, S_t gradually increases, and eventually the phase ends when $S_t \sim 1$, then the aggregates decouple from the turbulent gas. At this time, the mass and size of the aggregates become $m_d \sim 10^5$ g and $a_d \sim 100$ m, respectively. Their internal density is still very low (i.e., ‘‘fluffy’’).

In the next gravitationally compression phase, the aggregates are compressed owing to their self-gravity, and their internal density increases as $\rho_{int} \propto m_d^{0.4}$ (Kataoka et al. 2013). The relative velocity of the aggregates in this phase is determined by the energy balance among gravitational scattering, collisional energy loss, turbulent stirring, turbulent scattering and gas drag (Michikoshi, & Kokubo 2016, 2017) (see also Appendix). The aggregates finally grow to \sim km-sized bodies (i.e., planetesimals).

The value of the critical velocity for collisional destruction of cm to km sized dust aggregates is not clear. Numerical experiments of collisions between aggregates (Wada et al. 2009) showed that the critical velocity is 50-100 m s⁻¹ for $\sim 10^4$ monomers ($m_d \sim 10^{-11}$ g), and this scales with the mass of the aggregates as $\propto m_d^{1/4}$. If the critical velocity simply scales, it should exceed 1 km s⁻¹ for km-sized ‘planetesimals’.

In the regime with $S_t > 1$, if the Toomre Q -value for the disk of aggregates becomes smaller than ~ 2 , the gravitational instability takes place (e.g. Goldreich, & Ward 1973), and spiral density enhancements are formed, and it leads to rapid growth of planetesimals in a rotational period $t_K \equiv 2\pi/\Omega_K \simeq 9.5 \times 10^4 \text{ yr} (M_{BH}/10^6 M_\odot)^{-1/2} (r/1 \text{ pc})^{3/2}$ (see also Michikoshi, & Kokubo 2017). In fact, we found that the aggregate disks become gravitationally unstable soon after S_t reaches unity in most cases.

3. A TYPICAL EVOLUTION TRACK TOWARD PLANETS

We investigated the evolution of icy dust particles based on the processes explained in §2 to see if the four evolution stages of the dust aggregates are completed, by changing the parameters, such as the black hole mass M_{BH} , and turbulent viscous parameter α . The circumnuclear cold gas disk embedded in the geometrically thick torus (see Fig. 1) is assumed to be gravitationally stable. We assign a constant Toomre's Q -value, i.e. $Q_g = 2$ with the gas temperature $T_g = 100 \text{ K}$ in the disk³. The hydrogen column density of the gas disk is therefore $N_H \simeq 6.2 \times 10^{23} \text{ cm}^{-2} (M_{BH}/10^6 M_\odot)^{1/2} (r/1 \text{ pc})^{-3/2} (T_g/100 \text{ K})^{1/2}$. The gas mass between $r = 0.1 \text{ pc}$ and 10 pc in the thin disk is $M_g \simeq 5.7 \times 10^4 M_\odot (M_{BH}/10^6 M_\odot)^{1/2} (T_g/100 \text{ K})^{1/2}$. The total gas mass in the whole torus system of tens parsecs could be comparable to M_{BH} , as suggested by recent ALMA observations (Izumi et al. 2018; Combes et al. 2019).

Figure 2a shows a typical evolution of a dust aggregate at $r = 5.5 \text{ pc}$, just outside of the snow line ($r_{snow} = 4.7 \text{ pc}$) around a low luminosity AGN with $M_{BH} = 10^7 M_\odot$ and the Eddington ratio, i.e. the luminosity ratio to the bolometric luminosity, $\gamma_{Edd} = 0.01$. The internal density of the aggregate ρ_{int} is plotted as a function of its mass m_d . Here, we assume $\alpha = 0.1$. The internal density decreases monotonically from the monomer's density, $\rho_0 = 1 \text{ g cm}^{-3}$ to $4 \times 10^{-6} \text{ g cm}^{-3}$, as its mass increases from $m_d \sim 10^{-15} \text{ g}$ to $\sim 10^{-5} \text{ g}$. At that instant, the size of the aggregate becomes $\sim 0.1 \text{ cm}$. After this hit-and-stick phase, the fluffy dust aggregates keep growing by collisions in the turbulent gas motion until $S_t \simeq 1$. During this phase, the aggregates are compressed by the collisions, and therefore ρ_{int} gradually increase during this phase ($m_d = 10^{-6} \text{ g}$ to 10^5 g). At the end of this phase, their size become $a_d \sim 1 \text{ km}$. After this stage, the aggregates are compressed by their self-gravity, therefore ρ_{int} increases quite rapidly as seen below.

Figure 2b plots collisional velocity Δv of the aggregate [cm s^{-1}] and its size a_d [cm] as a function of m_d . a_d monotonically increases for $S_t < 1$. Initially Δv is 50 cm s^{-1} and it decreases in the hit-and-stick phase, after which it increases from 10 cm s^{-1}

³ Although $Q_g < 1$ is the necessary condition for the gravitational instability for the $m = 0$ mode perturbation in a thin, uniform disk, the non-axisymmetric modes can be unstable for $Q_g \lesssim 1.5$ (e.g. Laughlin, & Bodenheimer 1994). Therefore it is safe to assume $Q_g \sim 2$ for a gravitationally stable disk (see also Wada, & Norman 1999; Wada et al. 2002, where the effective Q -value is $\gtrsim 2$ in the multi-phase, quasi-stable gas disk).

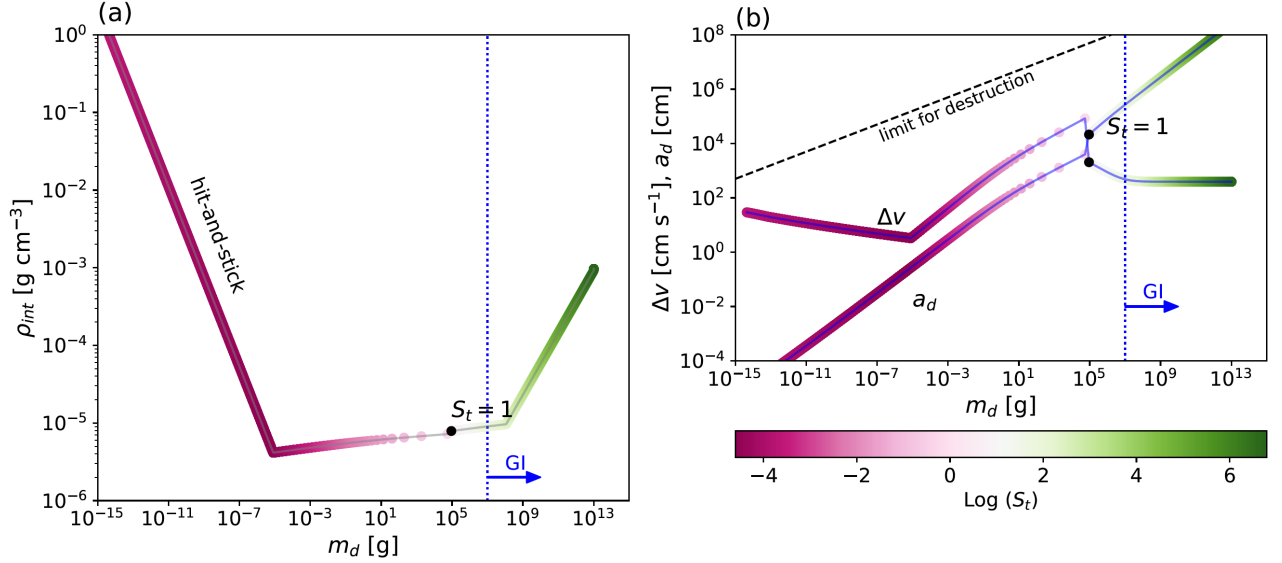


Figure 2. (a) Evolution of the internal density of a dust aggregate ρ_{int} as a function of the aggregate mass m_d for $M_{BH} = 10^7 M_\odot$, $\alpha = 0.1$ and the Eddington ratio is 0.01 (the bolometric luminosity of the AGN is 10^{43} erg s $^{-1}$), temperature of the gas $T_g = 100$ K. The dust sublimation radius is located at $r_{sub} = 0.3$ pc and the snow-line is $r_{snow} = 4.7$ pc. This plot for the dust at $r = 5.5$ pc. The aggregates grow by the hit-and-stick process, where the internal density of the aggregates monotonically decreases, that means the aggregates are porous in this phase. After the collisional energy exceeds critical energy, the aggregates start to get compressed ($m_d > 10^{-5}$ g). The color bar represents the Stokes number. For $S_t \sim 1$ the dust aggregates are decoupled from the gaseous turbulence.

(b) Collision velocity of the aggregates Δv and size of the aggregate a_d as a function of m_d . The dashed line shows the limit for the collisional destruction of the aggregates estimated from numerical experiments (Wada et al. 2009). After $S_t = 1$ is attained, Δv drops and the disk of the aggregates becomes gravitationally unstable to form more massive “planets”, shown by the vertical blue dotted line with “GI” (gravitational instability).

to ~ 500 m s $^{-1}$ around $S_t = 1$ in the collisional compression phase. It is far below the limit of the collisional destruction velocity of aggregates extrapolated from the numerical experiments of collisions between porous aggregates (Wada et al. 2008), which scales with the mass as $m_d^{1/4}$.

Figure 3 shows time evolution of ρ_{int} , a_d and Δv for the same model in Fig. 2. The hit-and-stick phase and the collisional compression phase take $\sim 3.8 \times 10^8$ yr. Soon after the aggregates are decoupled from gaseous turbulence, where $S_t \simeq 1$, their evolution is determined by various heating and dissipation (i.e., cooling) processes in the N -body system of the aggregates (Michikoshi, & Kokubo 2017). Note that Fig. 3b depicts a_d grows up to ~ 1000 km, but this does not happen because of the gravitational instability after $S_t = 1$. Fig. 3c shows that the collisional velocity Δv increases rapidly around $S_t \sim 1$, resulting in the rapid growth of the aggregates in the mass and density. The collisional velocity then dramatically decreases to ~ 4 m s $^{-1}$ due to collisional loss of their kinematic energy. This reduces the Toomre’s Q -value of the dust disk, and as a result $Q_d < 2$ is attained, therefore the system of km size aggregates becomes gravitationally unstable (denoted by the dotted lines with “GI” in

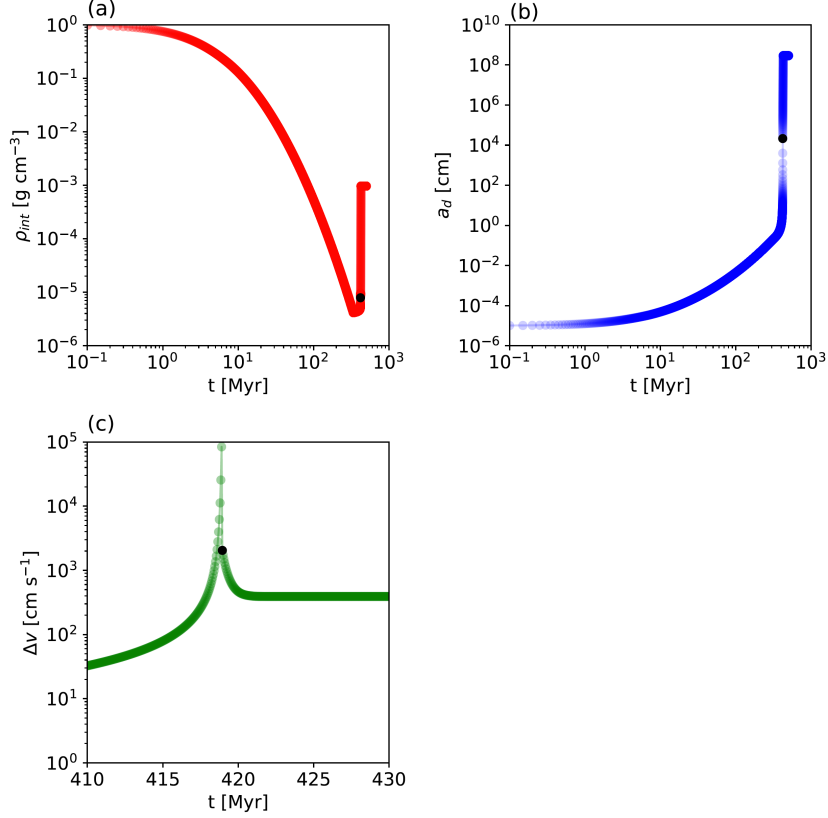


Figure 3. Time evolution of the internal density of the aggregate ρ_{int} , size a_d and relative velocity Δv for the same model shown in Fig. 2. The position where $S_t = 1$ is shown by filled circles.

Figs. 2a and 2b). This leads formation of spiral instabilities and their fragmentation followed by collapsing massive “planets” consisted of dust. This final unstable phase occurs very quickly with a few rotational period (i.e. 4×10^5 yr at $r = 5.5$ pc for $M_{BH} = 10^7 M_\odot$). The mass of “planets” then would be $m_{pl} \sim \lambda_{GI}^2 \Sigma_d \sim 10 M_E$, where λ_{GI} is the most unstable wavelength for the gravitational instability, and M_E is the Earth mass. In this model, the total number of the “planets” outside the snow line ($r = 4.7$ pc) to $r = 7$ pc is about 8.5×10^4 and its number density is $\Sigma_{planet} \sim 10^3$ pc $^{-2}$.

4. DISCUSSION

We then explored the evolution of the aggregates by changing α and M_{BH} . In Fig. 4, we plot time for which S_t becomes unity as a function of α and M_{BH} . The behavior of the dust growth is basically the same as the model with $M_{BH} = 10^7 M_\odot$ and $\alpha = 0.1$ (Figs. 2 and 3), but the time scale to reach the state with $S_t = 1$ depends on α and M_{BH} . For example, for $M_{BH} = 10^6 M_\odot$ and $\gamma_{Edd} = 0.01$, the snow line is located $r = 1.4$ pc. At $r = 2$ pc, it takes 2.6×10^8 yr when S_t exceeds unity. As shown in eq. (5), the growth time scale is proportional to $\alpha^{-1/2} H_g$, and $H_g \propto M_{BH}^{-1/2} r^{3/2}$. The snow line scales as $r \propto L_{AGN}^{1/2} \propto M_{BH}^{1/2}$. Therefore, the growth

time scale depends on $\alpha^{-1/2}M_{BH}^{1/4}$. As shown in Fig. 4, the time scale becomes $\sim 10^8$ yr for $\log \alpha > -0.3$ and $M_{BH} = 10^6 M_\odot$ or $\log \alpha > -0.2$ and $M_{BH} = 10^7 M_\odot$. In other words, formation of “planets” can be expected around the circumnuclear gas disks in *low luminosity Seyfert-type AGNs* rather than quasar-type high luminosity ones with massive SMBHs.

The growth time of an aggregate is proportional to $\alpha^{-1/2}$. Therefore, if α in the circumnuclear disk is as small as in the protoplanetary disks, i.e. $\alpha \sim 10^{-3} - 10^{-4}$, the growth time would be $6 \times 10^8 - 2 \times 10^9$ yr, which is still smaller than the cosmological time. However, because α is proportional to the mass accretion rate (eq.(6)), the Eddington rate of the central source as a result of the accretion would be $\gamma_{Edd} \sim 10^{-4} - 10^{-5}$, which corresponds to very low luminosity AGNs (e.g. Ricci et al. 2017). These imply that the planets could be also formed within a few giga-years around very faint AGNs.

The dust-to-gas mass ratio is assumed to be a standard value, i.e., 0.01 (Draine 2011), however this could be larger by few factors in the high metallicity environment (e.g. $\sim 4Z_\odot$) around AGNs (Groves et al. 2006; Rémy-Ruyer et al. 2014). In such case, the time scale of the dust evolution can be smaller by few factors than shown in Fig. 4.

Observing planets around SMBHs should be challenging. The standard techniques to detect exoplanets around stars, i.e., Doppler spectroscopy, transit photometry, gravitational micro-lensing, or direct imaging are hopeless. Photometry by a hard X-ray interferometer in space might be a possible solution, but the occultation of the accretion disk by the “planets” would be hard to distinguish from the intrinsic time variability of AGNs. The other, indirect way is detecting spectral changes in the *mm*-wave length due to opacity variation associated with the dust growth as used in protoplanetary disk. The opacity is roughly proportional to $\rho_{int} a_d$, and this increases by more than two orders of magnitude around $S_t \sim 1$.

ACKNOWLEDGMENTS

We would like to appreciate the anonymous referee’s valuable comments. This work was supported by JSPS KAKENHI Grant Number 18K18774. The authors thank Akio Inoue and Tohru Nagao for suggestions on metallicity and the dust-to-gas ratio in AGNs.

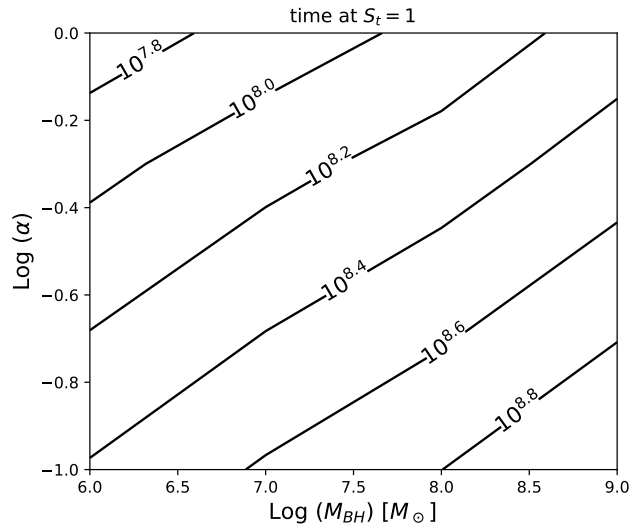


Figure 4. Evolution time [yr] at the Stokes parameter S_t becomes unity as a function of M_{BH} and α -parameter (Shakura, & Sunyaev 1973). After $S_t \sim 1$ is attained, the km-sized aggregate system is decoupled from the gaseous turbulence, and it becomes gravitationally unstable, leading to the formation of “planets” within $\sim 10^6$ yr in this parameter range.

REFERENCES

- Antonucci, R. 1993, *ARA&A*, 31, 473
- Barvainis, R. 1987, *ApJ*, 320, 537
- Buchner, J., Georgakakis, A., Nandra, K. et al. *A&Ap* 564, 125 (2014)
- Combes, F., García-Burillo, S., Audibert, A., et al. 2019, *A&A*, 623, A79
- Dominik, C., & Tielens, A. G. G. M. 1997, *ApJ*, 480, 647
- Draine, B. T. 2011, *Physics of the Interstellar and Intergalactic Medium* by Bruce T. Draine. Princeton University Press
- Draine, B. T., & Lee, H. M. 1984, *ApJ*, 285, 89
- Eisner, J. A., Hillenbrand, L. A., White, R. J., et al. 2007, *ApJ*, 669, 1072
- Event Horizon Telescope Collaboration, Akiyama, K., Alberdi, A., et al. 2019, *ApJL*, 875, L1
- García-Burillo, S., Combes, F., Ramos Almeida, C., et al. 2016, *ApJL*, 823, L12
- Goldreich, P., & Ward, W. R. 1973, *ApJ*, 183, 1051
- Groves, B. A., Heckman, T. M., & Kauffmann, G. 2006, *MNRAS*, 371, 1559
- Imanishi, M., Nakanishi, K., Izumi, T., et al. 2018, *ApJL*, 853, L25
- Izumi, T., Wada, K., Fukushige, R., et al. 2018, *ApJ*, 867, 48
- Kataoka, A., Tanaka, H., Okuzumi, S., et al. 2013, *A&A*, 557, L4
- Laughlin, G., & Bodenheimer, P. 1994, *ApJ*, 436, 335
- Marconi, A., & Hunt, L. K. 2003, *ApJL*, 589, L21
- Michikoshi, S., & Kokubo, E. 2017, *ApJ*, 842, 61
- Michikoshi, S., & Kokubo, E. 2016, *ApJL*, 825, L28
- Mukai, T., Ishimoto, H., Kozasa, T., et al. 1992, *A&A*, 262, 315
- Netzer, H. 2015, *ARA&A*, 53, 365
- Okuzumi, S., Tanaka, H., & Sakagami, M.-. aki . 2009, *ApJ*, 707, 1247
- Okuzumi, S., Tanaka, H., Kobayashi, H., et al. 2012, *ApJ*, 752, 106
- Ormel, C. W., & Cuzzi, J. N. 2007, *A&A*, 466, 413

- Rémy-Ruyer, A., Madden, S. C., Galliano, F., et al. 2014, *A&A*, 563, A31
- Ricci, C., Trakhtenbrot, B., Koss, M. J., et al. 2017, *Nature*, 549, 488
- Sato, T., Okuzumi, S., & Ida, S. 2016, *A&A*, 589, A15
- Schartmann, M., Wada, Keiichi, Prieto, M. A., Burkert, A., & Tristram, K. R. W. 2014, *MNRAS*, 445, 3878
- Shakura, N. I., & Sunyaev, R. A. 1973, *A&A*, 500, 33
- Shlosman, I., & Begelman, M. C. 1987, *Nature*, 329, 810
- Suyama, T., Wada, Koji, Tanaka, H., et al. 2012, *ApJ*, 753, 115
- Suzuki, T. K., Muto, T., & Inutsuka, S.-ichiro . 2010, *ApJ*, 718, 1289
- Tsukamoto, Y., Okuzumi, S., & Kataoka, A. 2017, *ApJ*, 838, 151
- Tristram, K. R. W., Burtscher, L., Jaffe, W., et al. 2014, *A&A*, 563, A82
- Wada, Koji., Tanaka, H., Suyama, T., et al. 2008, *ApJ*, 677, 1296
- Wada, K., & Norman, C. A. 1999, *ApJL*, 516, L13
- Wada, K., Meurer, G., & Norman, C. A. 2002, *ApJ*, 577, 197
- Wada, Keiichi. 2012, *ApJ*, 758, 66
- Wada, Keiichi. 2015, *ApJ*, 812, 82
- Wada, Koji., Tanaka, H., Suyama, T., et al. 2009, *ApJ*, 702, 1490
- Wada, Keiichi., Schartmann, M., & Meijerink, R. 2016, *ApJL*, 828, L19
- Wada, Keiichi., Fukushige, R., Izumi, T., & Tomisaka, K. 2018, *ApJ*, 852, 88
- Weidenschilling, S. J. 1977, *MNRAS*, 180, 57
- Youdin, A. N., & Lithwick, Y. 2007, *Icarus*, 192, 588

APPENDIX: EVOLUTION OF DUST AGGREGATED IN EACH STAGE

Here, we describe detail models of the dust evolution used in §3 and §4, based on the assumption that the elementary processes during the growth of the icy dust monomers to the planetesimals around stars can be applied to the dust particles in the circumnuclear disk around SMBHs. However, there are significant differences between the two systems (see Table 1), which could result in very different “planet” systems around SMBHs. The evolution of dust particles is divided into four phases as described below.

1. HIT-AND-STICK PHASE

If the dust aggregates grow by ballistic cluster-cluster aggregation (BCCA), the internal structure of the aggregate should be porous (i.e. $\rho_{int} \ll \rho_0 \sim 1 \text{ g cm}^{-3}$), and its fractal dimension is $D \simeq 1.9$ (Mukai et al. 1992; Okuzumi et al. 2009). In this case, the internal density of the aggregates in the hit-and-stick phase (Okuzumi et al. 2012; Kataoka et al. 2013) evolves as

$$\rho_{int} = (m_d/m_0)^{1-3/D} \rho_0, \quad (7)$$

where m_d is the mass of the aggregate, and m_0 and ρ_0 are the monomer’s mass and density, respectively. We assume that $m_0 = 10^{-15} \text{ g}$ and $\rho_0 = 1 \text{ g cm}^{-3}$. In contrast to the protoplanetary disk, the radial motions of the gas and dust are small. For example, the radial velocity of the gas disk for the Eddington ratio $\gamma_{Edd} = 0.1$ and the black hole mass $M_{BH} = 10^7 M_\odot$ is $10^{-4} v_K - 10^{-3} v_K$, where v_K is the Keplerian rotational velocity (see also eq.(3), (4)). Therefore, as the first approximation, we assume that the gas and dust surface density distribution ($\Sigma_d(r) = f_{dg} \Sigma_g(r)$) does not change during the evolution.

The growth rate for m_d is then

$$\frac{dm_d}{dt} = \frac{2\sqrt{2\pi} \Sigma_d a_d^2 \Delta v}{H_d}, \quad (8)$$

where a_d is the size of the dust aggregate, Δv is collisional velocity between the aggregates and H_d is the scale height of the dust disk given as (Youdin, & Lithwick 2007; Tsukamoto et al. 2017).

$$H_d = \left(1 + \frac{S_t}{\alpha} \frac{1 + 2S_t}{1 + S_t}\right)^{-1/2} H_g, \quad (9)$$

where $H_g = c_s/\Omega_K$ is the scale height of the gas disk.

The relative velocity between aggregates Δv for $S_t < 1$ can be divided into two regimes (Ormel, & Cuzzi 2007): regime I) $t_s \ll t_\eta = t_L Re^{-1/2}$, and regime II) $t_\eta \ll t_s \ll \Omega^{-1}$. The Reynolds number, $Re \equiv \alpha c_s^2 / (\nu_{mol} \Omega)$ with the molecular viscosity $\nu_{mol} \sim \frac{1}{2} c_s \lambda_g$ is

$$Re \approx 3 \times 10^4 M_{BH,6}^{-1/2} r_1^{3/2} c_{s,1}^{-1} Q_g \gamma_{Edd,0.01}, \quad (10)$$

where Q_g is the Toomre's Q -value for the gas disk. The eddy turn over time t_L is $t_L \sim \Omega_K^{-1}$, and $t_\eta \sim t_L$ for the smallest eddy. For the hit-and-stick phase, $S_t \ll R_e$, then Δv obeys the regime I, and

$$\Delta v_I \sim \sqrt{\alpha} c_s R_e^{1/4} |S_{t,1} - S_{t,2}| \sim \frac{1}{2} \sqrt{\alpha} c_s R_e^{1/4} S_t \quad (11)$$

$$\sim 0.5 \text{ [m/s]} \left(\frac{S_t}{1.5 \times 10^{-4}} \right)^{1/2} \left(\frac{\alpha}{0.3} \right)^{1/2} \left(\frac{R_e}{3 \times 10^4} \right) c_{s,1}, \quad (12)$$

where $S_{t,1}$ and $S_{t,2}$ are Stokes numbers of two colliding particles. We here assume $S_{t,2} \sim S_{t,1}/2$ (Sato et al. 2016). For regime II, on the other hand,

$$\Delta v_{II} \sim v_L \sqrt{t_{stop}/t_L} \sim \sqrt{\alpha S_t} c_s \quad (13)$$

$$\approx 6.7 \text{ [m/s]} \left(\frac{S_t}{1.5 \times 10^{-4}} \right)^{1/2} \left(\frac{\alpha}{0.3} \right)^{1/2} c_{s,1} \quad (14)$$

where v_L is velocity of the largest eddy.

The size of dust aggregates determines how they interact with the gas (e.g. the Stokes parameter is proportional to $\rho_{int} a_d$ for the Epstein law). Dynamics of the aggregates is affected by their cross sections, which depend on the internal inhomogeneous structure. The radius of BCCA cluster a_{BCCA} for large numbers of monomers N is given as $a_{BCCA} \simeq N^{0.5} a_0$ (Mukai et al. 1992; Wada et al. 2008, 2009), and this was also confirmed by N -body simulations (Suyama et al. 2012).

2. COLLISIONAL AND GRAVITATIONAL COMPRESSION PHASES

The hit-and-stick phase ends, when the rolling energy E_{roll} , which is the energy required to rotate a particle around a connecting point by 90° , is comparable to the impact energy, E_{imp} between the porous aggregates. Beyond this point, the aggregates start to get compressed by mutual collisions. Here, we assume $E_{roll} = 4.37 \times 10^{-9}$ erg (Suyama et al. 2012). When the number of monomers in the aggregates exceeds a critical number $N_{crit} \equiv \beta \frac{8E_{roll}}{m_0 \Delta v^2}$ with $\beta = 0.5$ (Suyama et al. 2012), they are compressed, and the internal density no longer decreases during the coagulation process.

The collisional velocity Δv between aggregates is determined by the interaction with the turbulence for $S_t < 1$, depending on S_t and R_e (Ormel, & Cuzzi 2007): For $S_t \leq R_e$,

$$\Delta v = \frac{1}{2} \sqrt{\alpha} c_s R_e^{1/4} S_t, \quad (15)$$

or for $S_t > R_e$,

$$\Delta v = \sqrt{\alpha S_t} c_s, \quad (16)$$

where $R_e \equiv \alpha c_s^2 / \nu_{mol} \Omega_K$ with the sound velocity of the gas disk c_s .

The internal density of the aggregated $\rho_{int,f}$ formed of two equal-mass aggregates, with density ρ_{int} , is calculated according to [Suyama et al. \(2012\)](#):

$$\rho_{int,f}^4 = \left(\rho_{int}^4 + \rho_0^4 \frac{E_{imp}}{0.15NE_{roll}} \right)^{1/4}. \quad (17)$$

As the aggregates become more massive for $S_t < 1$, they start getting compressed by their self-gravity, and the internal density evolves as $\rho_{int} \propto (\Delta v)^{3/5} m_d^{-1/5}$ ([Okuzumi et al. 2012](#)). This phase ends when the Stokes parameter becomes unity ($S_t \sim 1$). Then the aggregates are decoupled from the turbulent gas, and they evolve as N -body system.

3. EVOLUTION OF DUST AGGREGATES AS A N -BODY SYSTEM

When $S_t > 1$, the collisional velocity between the aggregates is determined by a balance between heating and cooling processes as the N -body particles. According to [Michikoshi, & Kokubo \(2016, 2017\)](#), we solve the following equation to get equilibrium random velocity of the dust aggregates v_d ,

$$\begin{aligned} \frac{dv_d^2}{dt} = & \left(\frac{dv_d^2}{dt} \right)_{grav} + \left(\frac{dv_d^2}{dt} \right)_{turb,stir} + \left(\frac{dv_d^2}{dt} \right)_{turb,grav} \\ & - \left(\frac{dv_d^2}{dt} \right)_{coll} - \left(\frac{dv_d^2}{dt} \right)_{drag} = 0. \end{aligned} \quad (18)$$

The first three heating terms are due to the gravitational scattering of the particles, stirring by turbulence, and gravitational scattering by turbulent fluctuation, respectively. The two cooling terms in eq.(18) represent the collisional damping and the gas drag.

4. GRAVITATIONAL INSTABILITY OF THE AGGREGATES DISK

We investigate gravitational instability (GI) of the disk consisted of the dust aggregate at $S_t > 1$ based on the Toomre's Q -value defined as $Q_d \equiv (v_d/\sqrt{3})\Omega_K/3.36G\Sigma_d$. For the axi-symmetric mode, $Q_d < 1$ is the necessary condition for the liner GI, but non-axisymmetric mode can be developed for $Q_d \lesssim 2$, and the spiral-like density enhancements are formed followed by fragment of the spirals ([Michikoshi & Kokubo 2017](#)), which leads formation of planets. The mass of the fragments can be estimated as $m_{pl} \simeq \lambda_{GI}^2 \Sigma_d$, where the critical wavelength for GI $\lambda_{GI} = 4\pi^2 G \Sigma_d / \Omega_K^2$. The number of "planets" then can be estimated as $N_{pl} \sim 2\pi r / \lambda_{GI}$. We found that the velocity dispersion of the aggregates drops rapidly due to the cooling terms in eq.(18). As a result, the system becomes gravitationally unstable after $S_t = 1$ in a rotational period.